journal

J. Am. Ceram. Soc., 93 [10] 3360–3369 (2010)
DOI: 10.1111/j.1551-2916.2010.03838.x

Engineering Photocatalytic Cements: Understanding TiO_2 Surface Chemistry to Control and Modulate Photocatalytic Performances

Andrea Folli,[†,‡] Isabelle Pochard,[§] André Nonat,[§] Ulla H. Jakobsen,[¶] Ashley M. Shepherd,[‡] and Donald E. Macphee[‡]

[‡]Department of Chemistry, University of Aberdeen, Aberdeen AB24 3UE, Scotland, U.K.

[§]Institut Carnot de Bourgogne, UNR 5209 CNRS, Université de Bourgogne, F-21078 Dijon, France

[¶]DTI, Byggeri–Beton, Gregersensvej, Høje Tåstrup DK-2630, Denmark

The present work addresses the aggregation/dispersion properties of two commercial titanias for application as photocatalysts in concrete technology. A microsized *m*-TiO_2 (average particle size 153.7 ± 48.1 nm) and a nanosized *n*-TiO_2 (average particle size 18.4 ± 5.0 nm) have been tested in different ionic media (Na^+, K^+, Ca^{2+}, Cl^-, SO_4^{2-}, synthetic cement pore solution) at different pHs and in real cement paste specimens. Results highlighted that ion–ion correlations play a fundamental role in TiO_2 particles aggregation in the cement environment. A particle aggregation model derived from TiO_2 surface chemistry is proposed here and used to justify such aggregation phenomena in real cement paste. Scanning electron microscopy–energy-dispersive X-ray spectroscopic investigations on hardened cement specimens completely confirmed the qualitative model based on titania surface chemistry. Experimental results also show how size and nature of TiO_2 aggregates dramatically influence the overall photocatalytic activity of cementitious materials containing TiO_2.

I. Introduction

Applications of TiO_2 photocatalysts to construction materials began toward the end of the 1980s. Two important effects related to the nature of photoactive TiO_2 coatings had by this time been discovered: (a) the self-cleaning effect due to redox reactions promoted by sunlight (or in general, weak UV light) on the photocatalyst surface,[1] and (b) the photo-induced hydrophilicity[2,3] of the catalyst surface, which enhances the self-cleaning effect (inorganics causing dirt and stains on surfaces can be easily removed due to rainwater soaking between the adsorbed substance and the TiO_2 surface). Photocatalytic glasses provide an example of self-cleaning and antifogging (wetting) properties.[4] Recently, photocatalytic cementitious materials have been patented.[5–10] The application of TiO_2 photocatalysis to concrete aims to achieve two main goals, the self-cleaning effect discussed above and the depolluting effect due to the oxidation of NOx in the atmosphere to NO_3^-, especially in street canyons where NOx concentrations can be considerable due to engine exhausts.[11–14] The great advantage provided by such products is that the only requirements, beyond TiO_2 in the construction material used, are sunlight and rainwater.

In the past 20 years, the large amount of literature about photocatalytic cementitious materials has predominantly dealt with efficiency issues. However, TiO_2 dispersion effectiveness and its influence on overall photocatalytic performances still lack systematic research. Few researchers investigated the effect of a Portland cement-like ionic environment on TiO_2 photocatalytic performance[15,16] (i.e., effect of Ca^{2+}, Na^+, K^+, and high pH, etc.) in slurry systems nor did they consider how titania surface chemistry could influence pollutant adsorption and its own dispersion in real cement structures. TiO_2 surface chemistry is the focus of the present paper. Titania ζ-potentials, surface charge densities (in presence of indifferent and nonindifferent electrolytes), chemical surface modifications, specific and nonspecific ion adsorptions, and particle size are discussed in relation to the stability and properties of TiO_2 dispersions in ionic media and in solid cement structures.

II. Experimental Procedure

(1) TiO_2 Samples

Throughout this study, two commercially available titanias: *m*-TiO_2 (microsized) and *n*-TiO_2 (nanosized), both in the 100% anatase form, have been used. These have been characterized in order to evaluate their main physical–chemical properties such as: light absorption characteristics, mineralogy, specific surface area, primary particle size, porosity, surface composition, ζ-potentials, and surface charge densities. Light absorption measurements were undertaken to derive the band-gap between valence band and conductance band and have been carried out on TiO_2 powder using UV diffuse reflectance spectroscopy (StellarNet EPP2000 Spectrometer, Tampa, FL). Spectra were analyzed and processed according to the Kubelka–Munk transform approach for indirect semiconductors.[17] X-ray diffraction (XRD) patterns were obtained using a Bruker D8 Advance diffractometer (Bruker AXS Inc., Madison, WI) equipped with a Cu$K\alpha_1$ 1.54 Å X-ray source operating at room temperature, in order to confirm crystallinity and polymorphism. Brunauer–Emmett–Teller (BET) [18]) specific surface areas (S_{BET}) were obtained by N_2 adsorption on powdered samples (after degassing at 150°C) using a Micromeritics ASAP 2020 (Norcross, GA). These data enabled the characterization of sample porosity as determined by the Barrett–Joyner–Halenda (BJH) model,[19] assuming cylindrical pores. Primary particle size evaluation was carried out by three different techniques: transmission electron micrographic (TEM) imaging (and further image analysis), XRD via the Scherrer equation, Eq. (1), and a simple geometrical model derived from the BET specific surface areas assuming the particles to be rigid spheres, Eq. (2).

$$d = \frac{0.9\lambda}{\mathrm{FWHM} \times \cos\theta_P} \quad (1)$$

$$d = \frac{6}{\rho_A \times S_{BET}} \quad (2)$$

G. Scherer—contributing editor

Manuscript No. 27313. Received December 30, 2009; approved March 31, 2010.
[†]Author to whom correspondence should be addressed. e-mail: a.folli@abdn.ac.uk

where λ is the X-ray wavelength = 1.54 Å, the full-width at half-maximum for anatase 101 peak, θ_P the Bragg diffraction angle for anatase 101 peak, ρ_A the density of anatase (3.895 g/cm^3), and S_{BET} is the BET specific surface area.

Investigations on the chemical nature of the sample surfaces have been carried out using both X-ray photoelectron spectroscopy (XPS) and scanning electron microscopy–energy-dispersive X-ray spectroscopy (SEM–EDS). X-ray photoelectron spectra have been obtained using a VG–Escalab (Thermo Fisher Scientific, Waltham, MA) X-Ray Photoelectron Spectrometer VGX900 (Al$K\alpha$ radiation) on the untreated sample powders. Spectral lines have been interpreted using the National Institute of Standards and Technology (NIST) database for XPS analysis[20] together with XI–SDP21 version 2.1 peak fitting software provided with the instrument. SEM–EDS micrographs and relative composition analyses have been carried out using an FEI Quanta 400 scanning electron microscope (Hillsboro, OR) equipped with a Thermo NSS-UPS-SEM-INORAN System SIX (Thermo Fisher Scientific, Waltham, MA) for X-ray microanalysis (EDS). Secondary electron images have been collected for the TiO_2 sample powders (no impregnation, no coating, low vacuum mode). EDS spectra have been analyzed using the database provided together with the instrument software.

The pH of zero charge (PZC) was evaluated by the zero change of pH consecutive to additions of an indifferent electrolyte. Sodium nitrate was used to increase the ionic strength from 10^{-3} to 10^{-2} mol/L of 1% w/w TiO_2 suspensions, in the pH range from 4 to 10 for *n*-TiO_2 and 1.7–10 for *m*-TiO_2. Simultaneously, the dynamic mobility of the particles was measured using a Colloidal Dynamics 7020 ZETAPROBE CAD apparatus (North Attleboro, MA).

Titration of the surface charge σ_0(pH) was made by measurements of the surface consumption of H^+ or OH^- by 252.5 g of 1% w/w TiO_2 suspension in 10^{-2} mol/L $NaNO_3$. Besides the suspension titration, the same procedure was applied to an identical volume of supernatant of the suspension. The H^+ or OH^- consumed by the surface at a given pH could be calculated from the difference in the amount of titrant (HCl or NaOH, both analytical grade) required for the supernatant solution and for the suspension to reach this given pH from the PZC. Namely, the total surface excess charge of the particle is computed from the following equation:

$$\sigma_0 = \frac{F}{mS_{BET}} C_T (V_{susp} - V_{super}) \quad (3)$$

where σ_0 is the surface excess charge in C/m^2, m is the mass of particles in g, S_{BET} is the BET specific surface area of the particles in m^2/g, F is the Faraday constant = 96 500 C/mol, C_T is the titrant concentration equal to 1 mol/L for both HCl and NaOH, and V_{susp} and V_{super} are the titrant volumes added at a given pH for the suspension and for the supernatant solution, respectively.

ζ-potentials were also measured for 1% w/w TiO_2 suspensions in calcium hydroxide solutions of various concentrations ranging from 0.05 to 16 mmol/L. Calcium concentrations in the solutions were determined using a VISTA-PRO VARIAN ICP optical emission spectrometer (Palo Alto, CA). Each sample was analyzed three times. The estimated error on the concentration was about 0.01 mmol/L.

(2) TiO_2 Dispersion Test

Dispersion tests have been carried out according to a procedure described in Jingxian *et al.*[21] The only difference is the amount of TiO_2 used, which in this work is about 2% m/v.

(3) Cement Pastes Preparation and SEM Investigation on TiO_2 Dispersion in the Cement Matrix

Cement specimens and relative SEM investigations, which this paper refers to, have already been used and described in one of the authors' previous papers.[22]

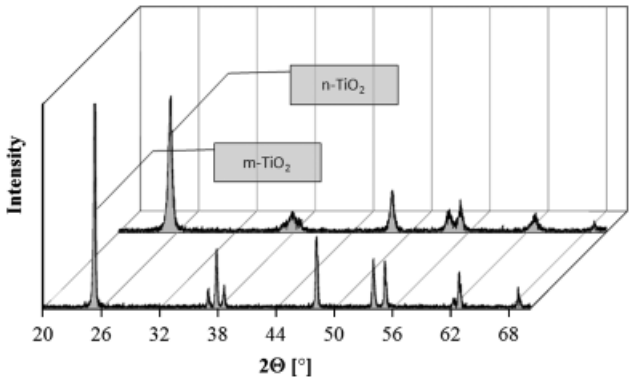

Fig. 1. X-ray diffraction patterns for both *m*-TiO_2 and *n*-TiO_2.

III. Results and Discussion

(1) Physical–Chemical Characterization of Commercial Photocatalysts

The results of XRD analyses are shown in Fig. 1. The peak positions confirm that both commercial TiO_2 products are essentially anatase.[23,24] Differences in the XRD patterns between the two samples (peak intensities and widths) are attributed to different particle sizes. Surface area data are presented in Fig. 2(a). The much lower level of N_2 adsorption on the microsized sample is consistent with this sample showing larger crystallites than the nanosized product. It is considered that the pore volume measured through the BJH analysis (Fig. 2(b)) on N_2 adsorption data is mainly related to the volume arising from particle agglomeration rather than intra particle pore volume. The corresponding porosity data cannot be obtained for the microsized sample as pore sizes are outside the measureable range.

Figure 3 shows TEM images of both products. Again, the crystallite size difference between the two samples is evident and this is quantitatively supported by the histograms shown as insets in the figure obtained by image analysis using more than one hundred particles for each samples. The above data are summarized in Tables I and II. There is good agreement between the techniques and the results are consistent with the manufacturers' data on particle size.

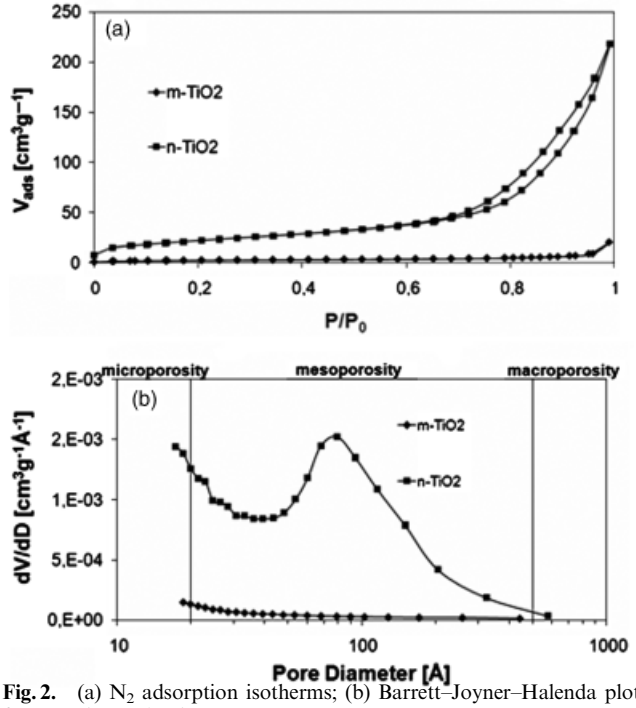

Fig. 2. (a) N_2 adsorption isotherms; (b) Barrett–Joyner–Halenda plot for porosity evaluation.

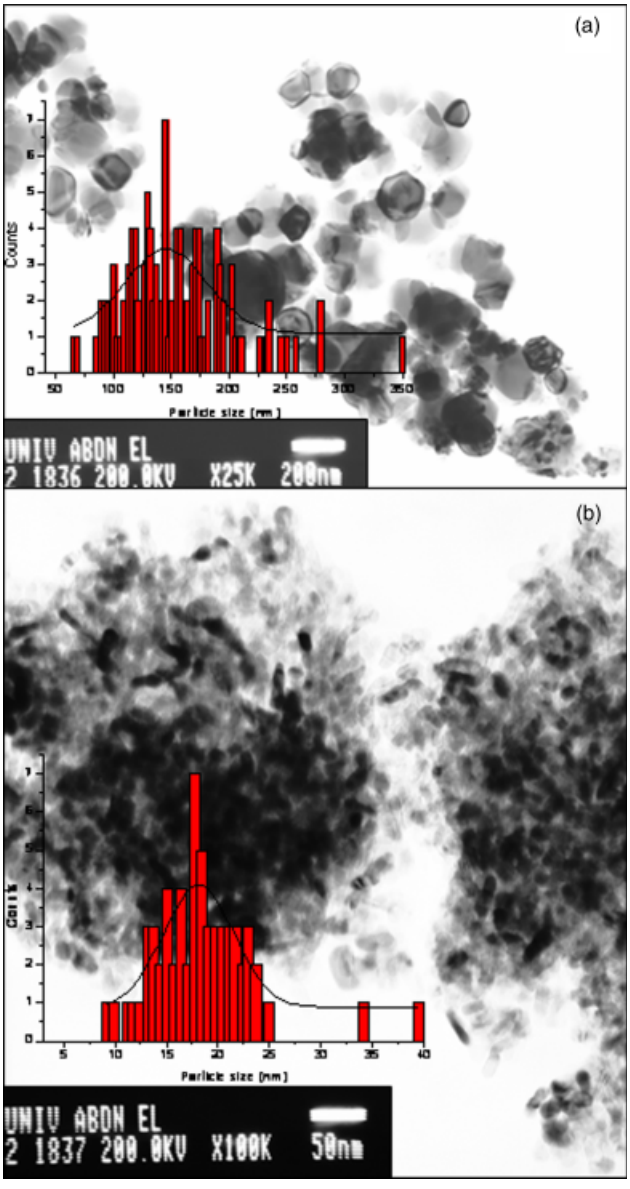

Fig. 3. Transmission electron micrographs and particle size distribution of: (a) m-TiO_2, (b) n-TiO_2.

Figure 4 shows XPS spectra of m-TiO_2 and n-TiO_2. The Ti $2p^{3/2}$ and Ti $2p^{1/2}$ peaks at 459.2 and 465.1 eV, respectively (doublet separation of about 5.9 eV) together with the satellite peak shifted by about 13.8 eV from the main Ti $2p^{3/2}$ peak, are typical of TiO_2.[25] The O 1s region is different for the two samples. n-TiO_2 showed a mean peak at 530.0 eV, evidence of an unmodified surface.[26] The shoulder around 532.0 eV means that the surface is partially covered with OH groups.[27,28] m-TiO_2 has an O 1s peak at about 531.0 eV and a shoulder around 533 eV. Nevertheless this signal appears to overlap with another small peak around 535.0 eV (see deconvolution in Fig. 4). The latter is not an unambiguous signal and could be attributed to the oxygen of various groups. Nevertheless, the peak at 535 eV could be attributed to P–O groups on the surface of m-TiO_2 due to the simultaneous presence at 133.4 eV of a P $2p^{3/2}$ peak, Fig. 5(a). Binding energies around 133–134 eV are typical of phosphorous bound to oxygen atoms. No phosphorous was detected on the surface of n-TiO_2. XPS analysis also revealed the presence of K for m-TiO_2 and traces of N for n-TiO_2., Figs. 5(b) and (c). Na and S were also detected, Figs. 5(d) and (e). This is characteristic for titanias produced according to the sulfate process. S comes from the raw materials used in manufacturing and Na from NaOH used to neutralize the hydrolysis product (i.e., acidic TiO_2 produced by the hydrolysis of $TiOSO_4$). SEM–EDS also revealed the presence of P and K for m-TiO_2. n-TiO_2 exhibited traces of K but no P at all, evidence that m-TiO_2 is specifically treated during manufacture with a phosphorous compound (not known). Small amount of Na and S have been found too and the amount of TiO_2 was above 98%$_w$ for both samples (EDS analysis).

Table I. TiO_2 Physical Characterization Data

Sample	Crystalline phase	Band gap (eV)	SBET (m^2/g)	BJH Φ_{pore} (Å)
m-TiO_2	100% anatase	3.29±0.02	8.7	Outside mesoporosity field
n-TiO_2	100% anatase	3.34±0.02	78.9	79.6

BET, Brunauer–Emmett–Teller; BJH, Barrett–Joyner–Halenda.

Table II. TiO_2 Particle Size Evaluation

Sample	Particle size (nm)		
	TEM (*a*)	XRD	BET
m-TiO_2	153.7±48.1	—	177.6
n-TiO_2	18.4±5.0	16.6±2.0	19.5

BET, Brunauer–Emmett–Teller; TEM, transmission electron micrography; XRD, X-ray diffraction.

Figures 6 and 7 show ζ-potential and surface charge density trends for the two titania samples investigated. ζ-potential trend for n-TiO_2 is typical for titania particles as reported by other authors.[29–31] The pH for which the ζ-potential equals zero, namely the iso-electric point (IEP), was found to be at pH 6.5. The PZC found for n-TiO_2 by the method of zero change of pH reads 6.5 too (see Fig. 7, surface charge density), indicating that the solution contains indifferent electrolytes only.[32,33] The IEP for m-TiO_2 was found at pH 2.1. The actual PZC is difficult to measure for m-TiO_2 because of the large variation of the titrant volume added for a small variation of pH at low pHs. However, the trend indicates also a similar value for the IEP; indeed, once again, the solution contains indifferent electrolytes only.

The ζ-potential of m-TiO_2 is clearly modified relative to that of n-TiO_2, essentially by chemical modification at the surface. The atypical ζ-potential trend, the high surface charge density, and the low IEP (pH = 2), can be interpreted together with XPS data. XPS identified P–O bonds on the m-TiO_2 surface. Nelson *et al.*[32] observed that specifically adsorbed phosphates on titanium dioxide surfaces shift the IEP from about pH 7 to 2. In the case of m-TiO_2, there is no specific adsorption of any phosphate so P–O groups must rather be part of the surface structure. It has become apparent that many commercial titanias[34] are treated with P compounds as precalciner additives. The thermal process allows foreign ions to move to the surface and become part of the final product surface structure. XPS also showed that surfaces are partially hydroxylated; therefore, really low IEP measured for m-TiO_2 (and the possible value of PZC suggested from the trend in Fig. 7) is likely to be associated with P–OH surface groups, with deprotonation starting at a much lower pH than for Ti–OH groups. Surface titanol groups, Ti–OH, are amphoteric and their ionization equilibria can be written as[35]:

$$Ti-OH_2^+ \overset{Ka_1^s}{\longleftrightarrow} Ti-OH + H^+ \quad (4)$$

$$Ti-OH \overset{Ka_2^s}{\longleftrightarrow} Ti-O^- + H^+ \quad (5)$$

with $pKa_1^s \approx 2.4$[35] and $pKa_2^s \approx 8$[35] (data for the nanosized Evonik Degussa P25 TiO_2, Evonik Industries AG, Essen, Germany). Surface titanol groups are in the Ti–OH form at a pH equal to

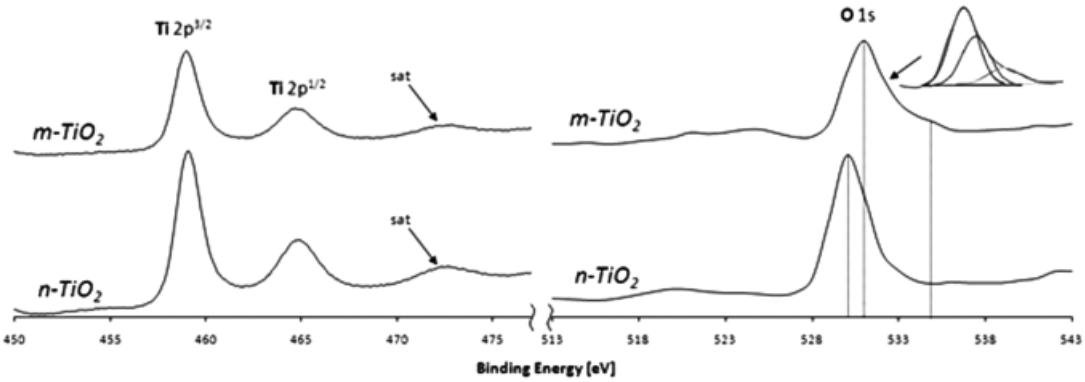

Fig. 4. *m*-TiO_2 and *n*-TiO_2 X-ray photoelectron spectroscopic spectra (Ti 2*p* and O 1*s* regions).

the PZC, which can be thermodynamically derived from the two acidic constants[35]:

$$\mathrm{PZC} = \frac{\mathrm{pKa}_1^s + \mathrm{pKa}_2^s}{2} \tag{6}$$

Equation (6) yields 6.25, very similar to the experimental value of 6.5 obtained by titration for *n*-TiO_2. At pHs lower than PZC, partial protonation of Ti–OH leads to positive Ti–OH_2^+ sites and at pHs higher than PZC partial deprotonation of Ti–OH leads to negative Ti–O^- sites (see Kormann *et al.*[35] for surface speciation). P–OH groups undergo similar mechanisms of protonation/deprotonation leading to positive and negative surfaces, but are much more acidic, accounting for the lower PZC of the P-containing *m*-TiO_2.

(2) m-TiO_2 and n-TiO_2 Dispersions in the Presence of Na^+, Cl^-, or Deionized Water

The stability of TiO_2 dispersions was tested in HCl, deionized water, and NaOH, pH = 2, pH = 7, and pH = 12.5, respectively. According to the DLVO theory,[36,37] dispersion/agglomeration of particles are controlled by the balance between attractive and repulsive forces. Because these systems contain only 1:1 electrolytes, a mean field approach is able to describe the electric double-layer interactions: repulsive contribution of entropic origin and attractive contribution resulting from van der Waals (VDW) forces. ζ-potential can therefore be used as a parameter to interpret/predict dispersion or aggregation phenomena. A common sedimentation test to verify dispersion stability[21] highlighted that: at pH = 2 in HCl, the *m*-TiO_2 dispersion is not stable and it readily sediments. At this pH, there is no net surface charge on the particles (IEP and PZC at pH = 2), interactions only come from attractive VDW forces; and hence, aggregation and sedimentation can be predicted. However, *n*-TiO_2 at the same pH shows a ζ-potential of about +20 mV (extrapolation of trend in Fig. 6 and Chen and colleagues[29–31]). This is enough to prevent sedimentation and the dispersion is perfectly stable not only at 24 h but also after 4 days. Furthermore, according to Mandzy *et al.*,[30] a potential of about |25–30| mV is the minimum threshold to *electrostatically stabilize* a *nanosized* TiO_2 dispersion (in presence of indifferent electrolytes only) mainly by breaking up big agglomerates, reducing their dimensions to primary particle size, and avoiding reagglomeration. At pH = 7 (deionized water), the situation is exactly the reverse. The PZC is nearer 7 for *n*-TiO_2 and hence its dispersion is unstable. *m*-TiO_2, having a ζ-potential of about −75 mV at this pH, provides a stable dispersion. At pH = 12.5 both of the samples show nonzero ζ-potentials: about −25 mV for *n*-TiO_2

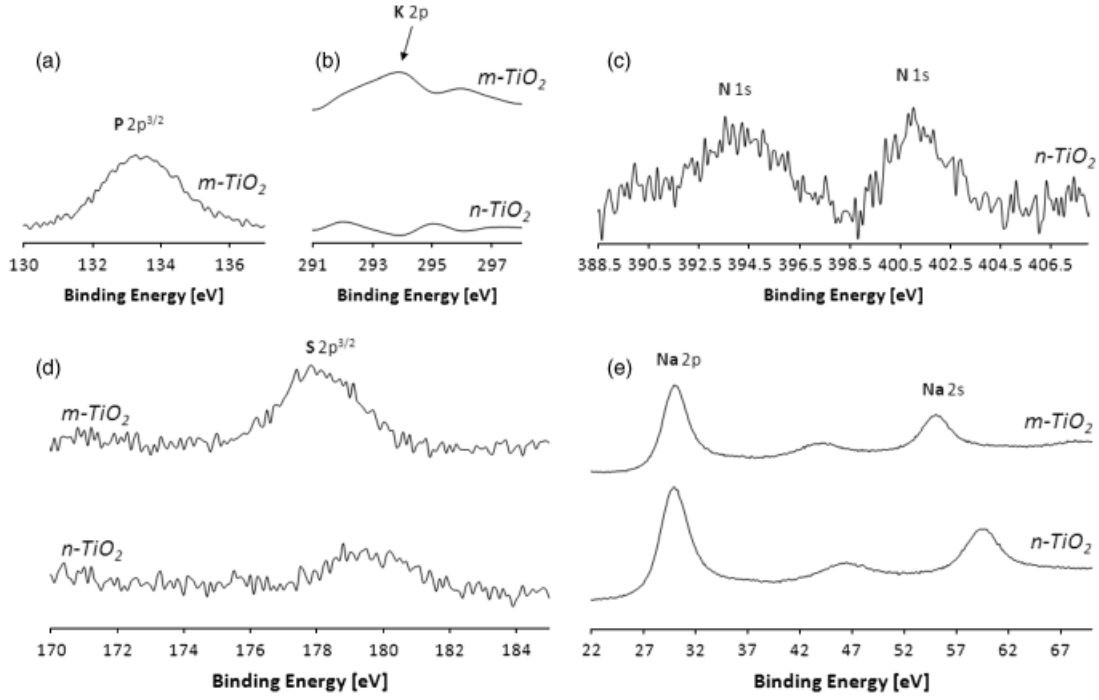

Fig. 5. *m*-TiO_2 and *n*-TiO_2 X-ray photoelectron spectroscopic spectra: (a) P $2p^{3/2}$ region; (b) K 2p region; (c) N 1s region; (d) S $2p^{3/2}$ region; and (e) Na 2p and 2s regions.

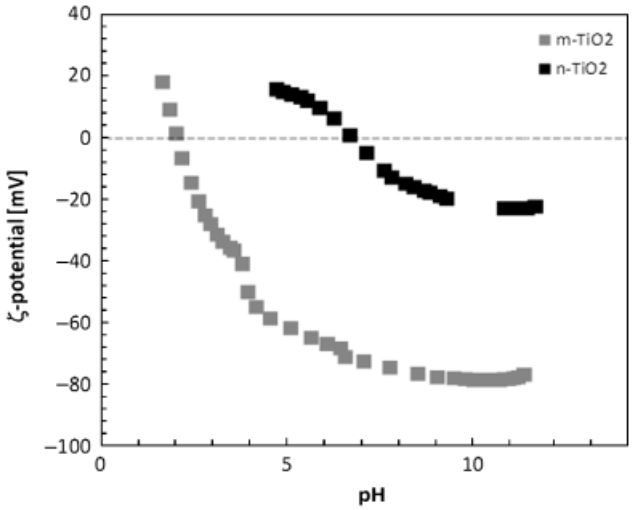

Fig. 6. *m*-TiO_2 and *n*-TiO_2 ζ-potentials vs pH 1% TiO_2 suspensions in 0.01*M* $NaNO_3$ solution.

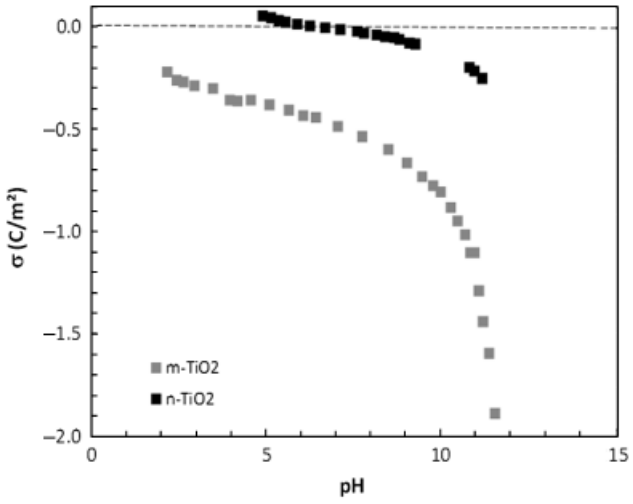

Fig. 7. *m*-TiO_2 and *n*-TiO_2 surface charge densities.

and about −80 mV for *m*-TiO_2 (Fig. 6), and as expected are highly dispersed with no significant differences in stability within 24 h. However, after 4 days *m*-TiO_2 looked better dispersed than *n*-TiO_2. This difference is likely associated with its higher ζ-potential, which is able to compensate the greater VDW attractive interaction.

(3) m-TiO_2 and n-TiO_2 Dispersions in the Presence of K^+

The same dispersions of *m*-TiO_2 and *n*-TiO_2 at pH = 12.5 have been prepared using a KOH solution. The potassium ion is considered to be an indifferent electrolyte too (no specific adsorption inside the Stern layer) but it is less polarizing than sodium. Its hydration shell is smaller and weaker than the sodium one (see Table III), and as a result, stronger interactions between hydrated K^+ ions and TiO_2 surface may occur. According to Shaw,[33] K^+ is expected to slightly destabilize colloidal suspensions. Monovalent electrolytes may increase flocculation according to their hydrated ionic radii.[33] The smaller the solvated ionic radius the closer the counter-ion approaches the particle surface and the stronger the resulting interaction. Thus, monovalent cations can be arranged in a series of decreasing flocculating power (increasing solvated radius, see Table III). This has been observed to be true for *n*-TiO_2 where, although within 24 h no particular differences with the Na^+ case have been noticed, after 4 days titania powder completely settled in KOH while the same dispersion in NaOH was still highly stable. For *m*-TiO_2, the observed situation is again totally different. The ζ-potential trend in Fig. 6 is still valid because in solution there are just indifferent electrolytes, and hence high dispersion stability is expected due to the high ζ-potential value. However, this dispersion settled within 1 h. A specific interaction between the high potassium activity environment and the P, K modified surface of *m*-TiO_2 appears to exist, even though the nature of such an interaction is not completely clear and further investigations might be needed.

(4) m-TiO_2 and n-TiO_2 Dispersions in the Presence of Ca^{2+}

Divalent (and even more, trivalent) cations are known to decrease colloidal stability (increasing flocculation).[38] Their higher charge makes them more polarizing than monovalent cations and the coulombic attraction between the divalent cations and the negatively charged surface, as well as the coulombic repulsion among the cations themselves, are greater than in the case of monovalent ions; this results in the so-called ion–ion correlations in the electrical double layer. In the conditions of high surface charge densities and in the case of multivalent counterions (highly coupled systems), ion–ion correlations can be at the origin of surface *overcharging* phenomena, and apparent surface charge reversal (CR).[39–41] They introduce an attractive electrostatic contribution between particles with the same charges.[42] Such phenomena have been demonstrated by many authors working on different colloidal systems and have been confirmed by several simulations[15,43–48] as identified in two recent reviews.[49,50] Labbez *et al.*[39] recently achieved important results with the quantification of such charge correlations for colloidal silica dispersions.

These effects on different TiO_2 samples have been proved here. Experimental results confirmed first evidences of TiO_2 CR in the presence of Ca^{2+} discussed by Mange *et al.*[15] and Böhmer *et al.*[51] Moreover, the charge correlations effects observed can be used to explain TiO_2 aggregation/dispersion in real cement structures.

ζ-potential measurements performed on *m*-TiO_2 and *n*-TiO_2 at different Ca^{2+} activities showed different trends to those for the Na^+ case, Fig. 8. As mentioned before, in alkaline conditions *n*-TiO_2 titanol groups are partially ionized to $Ti–O^-$ leading to a negative surface charge. Increasing calcium concentrations decrease the absolute value of ζ-potential until Ca^{2+} ions completely balance the surface charge and the overall potential at the shear plane is zero. *This new IEP is not at the PZC*. Although the actual TiO_2 surface is still negatively charged, the net charge at the shear plane is zero due to negative/positive charge compensation. With further increase in calcium concentration, the surface attracts counter-ions in excess of its own nominal charge[39] and the net charge detected at the shear plane

Table III. Data on Hydration of Aqueous Group IA Ions and NH_4^+

	Cs^+	≈	Rb^+	<	NH_4^+	≈	K^+	<	Na^+	<	Li^+
Hydrated ionic radius (Å)	2.28[58]		2.28[58]		≈2.32[58]		2.32[58] 3.31[59]		2.76[58] 3.58[59]		3.40[58]
Approximate hydration numbers	9.9[58] 6[60]						10.5[58] 7[60]		16.6[58] 13[60]		25.3[58] 22[60]
Hydration enthalpy (kJ/mol)	264[58]		293[58]				322[58] 295[61]		406[58] 365[61]		519[58]

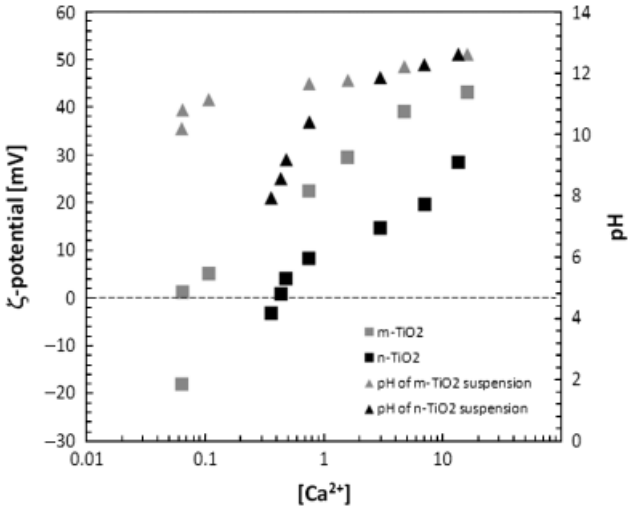

Fig. 8. m-TiO_2 and n-TiO_2 ζ-potentials vs $[Ca^{2+}]$.

is now positive and indeed the ζ-potential reversed (Fig. 8). OH^- ions in the diffuse layer balance the excess of the positive charge. Ion–ion correlations are responsible for this overcharging and subsequent CR here.[39,51]

For m-TiO_2, the process is analogous but, once again, the ionization chemistry of the surface is affected by the presence of P–OH and not driven by Ti–OH groups only. This, together with the much smaller specific surface area, is responsible for the different IEP.

Dispersions prepared for both m-TiO_2 and n-TiO_2 at pH = 12.5 in $Ca(OH)_2$ solutions revealed a high instability although both the systems were far away from their own IEPs. The high level of aggregation induced by the Ca^{2+} ions is also confirmed by the good transparency of the supernatant liquid after complete sedimentation. This is the consequence of the attractive electrostatic interactions promoted by ion–ion correlations, already observed also for C–S–H (calcium silica hydrate gel) particles.[42,44,45]

(5) m-TiO_2 and n-TiO_2 Dispersions in the Presence of SO_4^{2-}

The stability of TiO_2 systems at pH = 2 in presence of SO_4^{2-} ions (H_2SO_4 solution) has been found to be very similar to the case of Ca^{2+}. Phenomena described in the previous section can be used again here to interpret the experimental evidence of dispersion-reduced stability.

(6) m-TiO_2 and n-TiO_2 Dispersions in the Presence of Na^+, K^+, Ca^{2+}, and SO_4^{2-}, i.e., Synthetic Cement Pore Solution

The synergistic effect of all the ions discussed previously has been studied for titania dispersions in an ionic soup used to model the cement pore solution. The composition of the synthetic pore solution according to Houst *et al.*,[52] is given in Table IV and accounts for a measured pH of 12.87 ± 0.02. Neither of the two dispersions is stable in this ionic solution and a significant sediment is formed even after 10 min only (similar to the H_2SO_4 and $Ca(OH)_2$ systems as expected). Figure 9 shows the appearance of such dispersions from 10 to 30 min. The clarity of the supernatant solution and the height of the sediment give rise to interesting observations. After 10 min, m-TiO_2 showed a compact and small precipitate, that did not change significantly in volume with time. Furthermore, the supernatant solution did not appear totally clear both at 10 min and at

Table IV. Synthetic Cement Pore Solution Composition and pH

Ca^{2+} (mM)	Na^+ (mM)	K^+ (mM)	SO_4^{2-} (mM)	OH^- (mM)	pH
21.2	97.8	180.1	85.9	148.6	12.87 ± 0.02

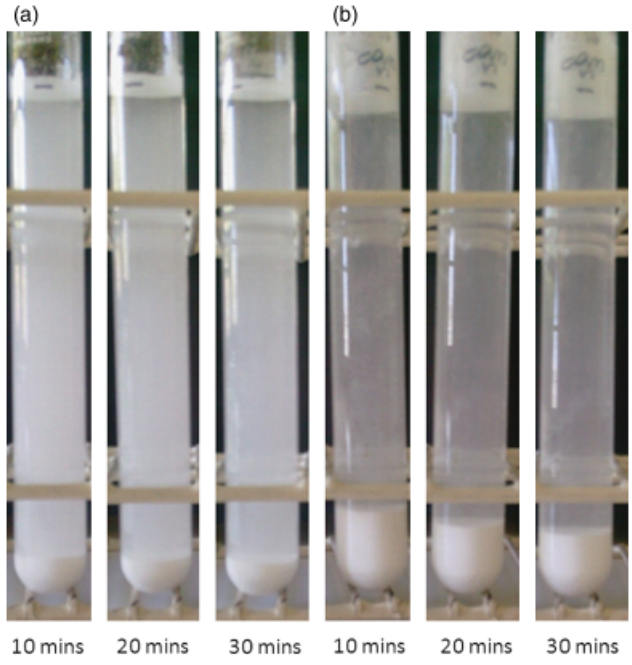

Fig. 9. Sedimentation test for: (a) m-TiO_2 and (b) n-TiO_2 in a synthetic cement pore solution (pH = 12.87).

longer times. According to Shaw,[33] this is evidence of small particle aggregates, which settle very compactly (small interaggregate volume) and leave the supernatant solution turbid due to even smaller aggregates kept dispersed by Brownian motion (*deflocculated* sediment). On the other hand, n-TiO_2 showed the opposite behavior. The higher level of sediment formed after 10 min which, reduced with time, and the clearer supernatant solution (at any time) suggest bigger particle aggregates. Their bigger size prevents a compact early stage settling (higher interaggregate volume and consequent higher sediment height). The volume of the sediment decreases in time due to space rearrangements caused by gravity. Nevertheless, the supernatant solution appears clearer at any time because the bigger aggregates are less affected by thermal motion (*flocculated* sediment). The graphical model describing these different sedimentation phenomena is shown in Fig. 10.

(7) TiO_2 Dispersion in Hardened Cement: A Particle Aggregation Model

Results obtained for TiO_2 dispersions in synthetic cement pore solutions can be used to predict the behavior and properties of the two different titanias in a real cement environment. During the preparation of cement paste specimens, cement, water, and

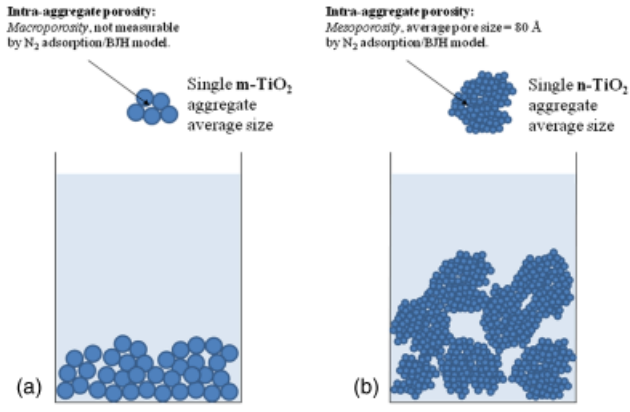

Fig. 10. Flocculating/deflocculating sedimentation model. (a) m-TiO_2, deflocculated sediment; (b) n-TiO_2, flocculated sediment.

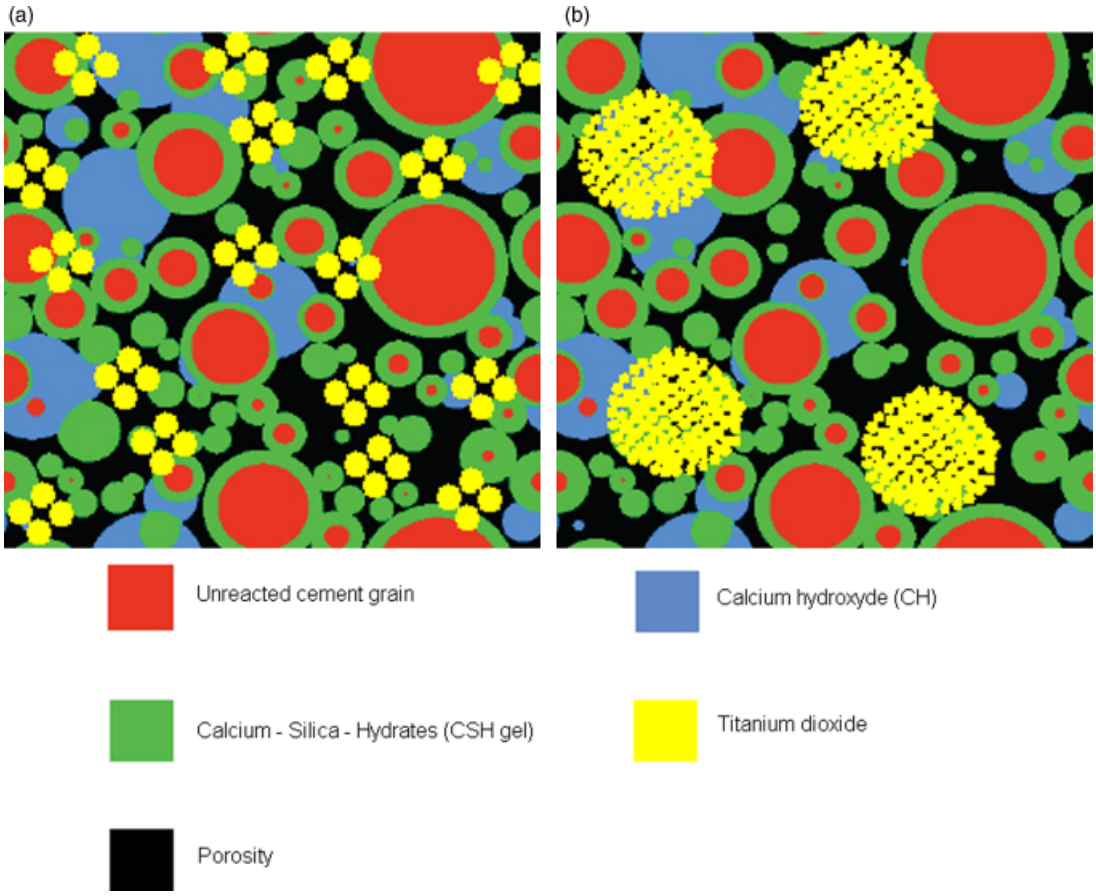

Fig. 11. Hardened cement structures with: (a) *m*-TiO_2 and (b) *n*-TiO_2.

TiO_2 are mixed together by mechanical stirring as described in the experimental section. Hydration of cement powder quickly produces a liquor with composition and pH very similar to the ion soup taken into account previously. In such conditions, considering also that TiO_2 does not take part in any of the chemical reactions forming cement hydrated phases, it is assumed that *m*-TiO_2 and *n*-TiO_2 undergo aggregations as described in the previous section. Mechanical stirring distributes particle aggregates all over the forming material. Once the cement has completely hardened, the dispersion of the two TiO_2s can be predicted according to the model shown in Fig. 11. For an equal mass of TiO_2 introduced into cement, *m*-TiO_2 is expected to have smaller and better dispersed aggregates than *n*-TiO_2 for which aggregates are bigger and more difficult to spread.

Validation of this qualitative model has been carried out by SEM–EDS investigation on real cement paste specimens containing either *m*-TiO_2 or *n*-TiO_2. Micrographs in Fig. 12 were obtained for the surface layer of the cement samples (1 day cured) prepared with *m*-TiO_2 (Fig. 12(a)) and *n*-TiO_2 (Fig. 12(b)) while micrographs in Fig. 13 are of sections cut perpendicularly to the surface and show the layers beneath the surface. Surface micrographs (Fig. 12) show a higher degree of *m*-TiO_2 dispersion (white spots in Fig. 12(a)). Cement prepared with nanosized *n*-TiO_2 shows larger particle aggregates (a lower degree of dispersion (see Fig. 12(b))). This is especially evident

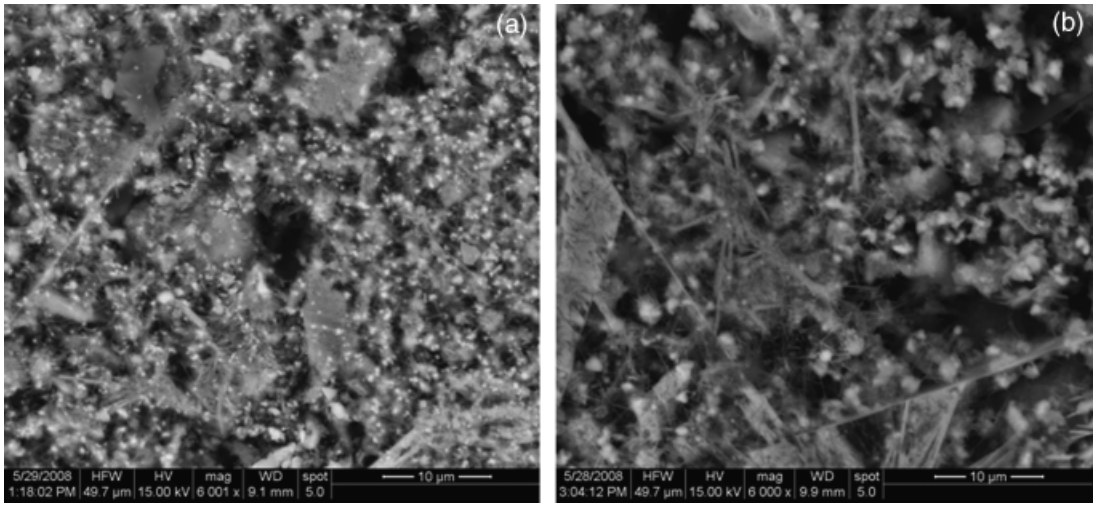

Fig. 12. Scanning electron microscopic surface micrographs for cement specimens (1 day cured) prepared with: (a) *m*-TiO_2, (b) *n*-TiO_2. SEM conditions adopted: no impregnation, no coating, low vacuum mode.

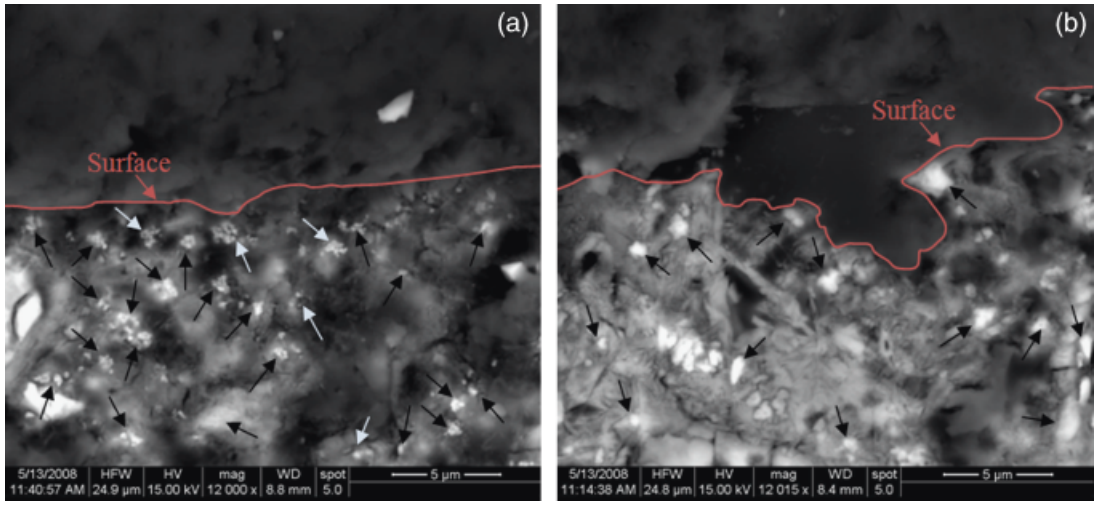

Fig. 13. Scanning electron microscopic (SEM)-polished cross-section micrographs for cement specimens (1 day cured) prepared with: (a) *m*-TiO_2, (b) *n*-TiO_2. SEM conditions adopted: impregnation,[56,57] no coating, low vacuum mode.

when the scale of the micrograph is considered. Nanoparticulate agglomerates appear to be at least 1 μm in dimension compared with *m*-TiO_2 agglomerates, which appear to be smaller and divided into smaller subagglomerates. A similar situation is achieved in the bulk of the specimens, Fig. 13. Figure 13(a), related to cement prepared with *m*-TiO_2, shows smaller and better dispersed TiO_2 particle aggregates compared with *n*-TiO_2-containing pastes, Fig. 13(b). These results, also illustrated as Ti-element maps (Fig. 14) of 14-day-cured cements, are in perfect agreement with the model proposed in Fig. 11.

(8) Impacts on Photocatalytic Performances

Knowledge acquired through the study of titania surface chemistry can be used to modulate the overall photocatalytic activity of Portland cement containing TiO_2. In simple slurry conditions

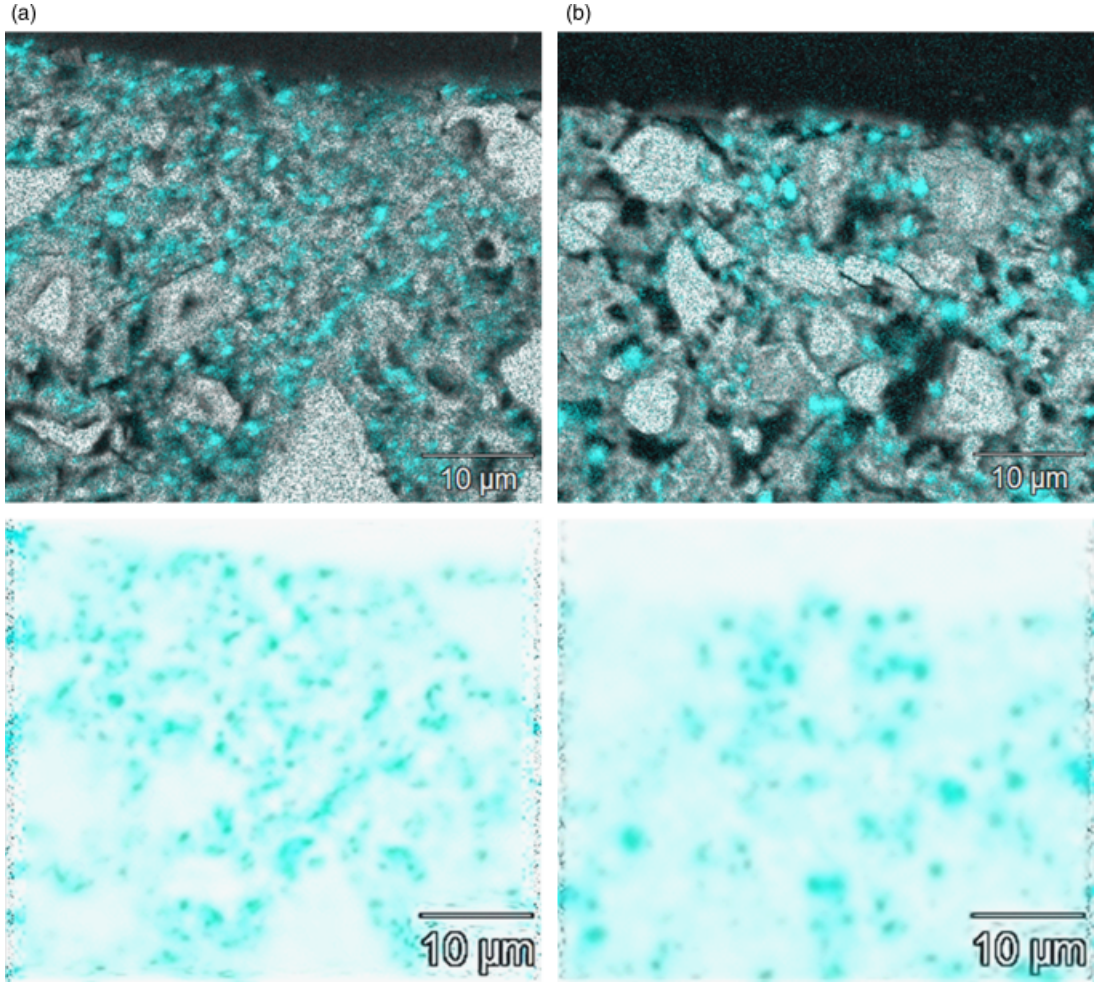

Fig. 14. Scanning electron microscopic (SEM)-polished cross-section micrographs for cement specimens (14 days cured) prepared with: (a) *m*-TiO_2, (b) *n*-TiO_2. SEM conditions adopted: impregnation,[56,57] C coating, high vacuum mode.

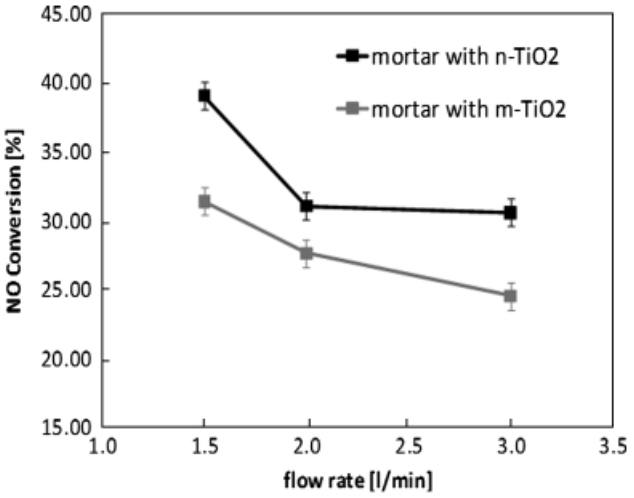

Fig. 15. NO conversion on Portland cement mortars containing TiO_2.

indeed, *n*-TiO_2 is supposed to perform better than *m*-TiO_2 due to its much higher specific surface area. This is not always true in solid materials like cement where TiO_2 is highly aggregated and the adsorption of target molecules depends on the 3D structure of the material, its porosity, and not least the TiO_2 aggregates porosity. In a previous work,[22] we highlighted that the degradation of Rhodamine B on the same cement specimens under UV light (a common test for the evaluation of the self-cleaning effect of photocatalytic concretes), was more efficient in the case of cement prepared with *m*-TiO_2 rather than *n*-TiO_2. On the other hand, preliminary studies on degradation of NOx (NO and NO_2)[53] in similar specimens with UV light, showed better results using *n*-TiO_2, Fig. 15. Large molecules like Rhodamine B, with an average molecular diameter of about 1.6 nm,[54] can penetrate only with difficulty the interior of an *n*-TiO_2 cluster (pore size around 8 nm), but readily can access *m*-TiO_2 clusters (see Table I). Moreover, RhB sticks on the cement specimen surface and does not penetrate inside the cement pore structure. The smaller and better dispersed *m*-TiO_2 clusters on the surface of the specimens (Fig. 12(a)) together with their macropores (Table I), offer a higher *available* surface area for adsorption and consequent reaction of big molecules like Rhodamine B than the bigger and poorly dispersed *n*-TiO_2 clusters. Conversely, gaseous NOx, due to the much smaller dimensions, 100–200 pm,[55] can easily penetrate both *m*-TiO_2 and *n*-TiO_2 clusters and the higher specific surface area for *n*-TiO_2 (measured by N_2 adsorption) obviously plays a key role as expected.

IV. Conclusions

Two commercial titania samples, both in the anatase form but with different average particle sizes, were investigated in efforts to understand their different photocatalytic properties when supported on a cement surface. *m*-TiO_2, with an average particle size of around 150 nm, was found to have surface P–OH groups. *n*-TiO_2, particle size around 17 nm, was not surface modified. The study has linked the aggregation/dispersion characteristics of the different samples with the size/surface chemistry through a discussion of ion–ion correlation forces and offers an explanation for the observed distribution and dispersion of the catalyst on the surface and in the near surface of real cement specimens.

Results in the ionic environment simulating cement pore solution revealed that both the titania sample particles undergo aggregation phenomena and produce unstable dispersions due to specific adsorbed ions on the TiO_2 surfaces. *m*-TiO_2 disperses due to its bigger primary particle size but mainly due to the P–OH surface modification. *n*-TiO_2 exhibits highly *flocculated* particle aggregates, leading to a much bigger secondary particle size (i.e., aggregate size). Based on these experimental observations, a model for the structure of TiO_2 particles in hardened cementitious matrixes is proposed, where *m*-TiO_2 is expected to be better dispersed and with smaller particle aggregates than *n*-TiO_2. SEM–EDS investigations on real cement specimens containing about 3.5% of TiO_2 (either *m*- or *n*-) validate the model.

The aggregation phenomena may also provide for the comparative performances of the two TiO_2 sample types in the photocatalytic degradation of Rhodamine B and NOx using cementitious specimens as a substrate. TiO_2 primary and secondary particle size, dispersion, and aggregate porosity in cement define the accessible surface area; big particle aggregate pores, small, and highly dispersed aggregates of *m*-TiO_2 offer a higher *available* surface area for adsorption and reaction of big molecules like Rhodamine B, which hardly penetrate *n*-TiO_2 particle aggregate pores. On the other hand, very small molecules like nitrogen oxides, which can easily penetrate into *n*-TiO_2 aggregate pores too, are better degraded by *n*-TiO_2. Indeed in this case, dispersion and aggregates porosity are not crucial; the available surface area is most likely to be due to the specific surface area determined by the primary particle size.

Acknowledgments

The authors are grateful to the European Community under the Marie Curie Research Training Network MRTN-CT-2005-019283 "Fundamental understanding of cementitious materials for improved chemical physical and aesthetic performance" (http://www.nanocem.org/MC-RTN/) for the full support of Andrea Folli.

The authors are also grateful to Dr. C. Labbez (Université de Bourgogne, Dijon Cedex, France) for the helpful discussions about stability of TiO_2 colloidal suspensions in highly coupled systems.

References

[1]A. Fujishima, K. Hashimoto, and T. Watanabe, *TiO_2 Photocatalysis: Fundamentals and Application*. BKC, Tokyo, 1999.

[2]H. Irie, T. Siew-Ping, T. Shibota, and K. Hashimoto, *Electrochem. Solid State Lett.*, **8**, 23–5 (2005).

[3]R. Wang, K. Hashimoto, A. Fujishima, M. Chikuni, E. Kojima, K. Kitamura, M. Shimohigoshi, and T. Watanabe, *Nature*, **338**, 431–2 (1997).

[4]D. W. Sheel, R. J. McCurdy, and S. J. Hurst, "Self-Cleaning Glazing Sheet"; WO Patent, 98/06675, 1998.

[5]L. Cassar and P. Carmine, "Hydraulic Binder and Cement Compositions Containing Photocatalyst Particles"; USA Patent, 6409821, 2002.

[6]R. Cucitore, S. Cangiano, and L. Cassar, "High Durability Photocatalytic Paving for Reducing Urban Polluting Agent"; WO Patent, 2006/000565, 2006.

[7]L. Cassar, R. Cucitore, and C. Pepe, "Cement-Based Paving Blocks for Photocatalytic Paving for the Abatement of Urban Pollutants"; Europe Patent, 1601626, 2005.

[8]Y. Murata, Yoshihiko, H. Tawara, H. Obata, and K. Murata, "NOX-Cleaning Paving Block"; Europe Patent, 0786283, 2003.

[9]L. Cassar, A. Beeldens, N. Pimpinelli, and G. L. Guerrini, "Photocatalysis of Cementitious Materials"; pp. 131–45 in *International RILEM Symposium on Photocatalysis, Environment and Construction Materials*, Vol. 1, Edited by P. Baglioni, and L. Cassar RILEM, Florence, 2007.

[10]G. L. Guerrini, A. Plassais, C. Pepe, and L. Cassar, "Use of Photocatalytic Cementitious Materials for Self-Cleaning Applications"; pp. 219–26 in *International RILEM Symposium on Photocatalysis, Environment and Construction Materials*, Edited by P. Baglioni, and L. Cassar RILEM, Florence, 2007.

[11]A. Beeldens, "Air Purification by Road Materials: Results of the Test Project in Antwerp"; pp. 187–94 in *International RILEM Symposium on Photocatalysis, Environment and Construction Materials*, Vol. 1, Edited by P. Baglioni, and L. Cassar. RILEM, Florence, 2007.

[12]G. L. Guerrini and E. Peccati, "Photocatalytic Cementitious Roads for Depollution"; pp. 179–86 in *International RILEM Symposium on Photocatalysis, Environment and Construction Materials*, Vol. 1, Edited by P. Baglioni, and L. Cassar. RILEM, Florence, 2007.

[13]M. Kawakami, T. Furumura, and H. Tokushige, "NOx Remediation Effects and Physical Properties of Cement Mortar Incorporating TiO_2 Powder"; pp. 163–70 in *International RILEM Symposium on Photocatalysis, Environment and Construction Materials*, Vol. 1, Edited by P. Baglioni, and L. Cassar. RILEM, Florence, 2007.

[14]C. S. Poon and E. Cheung, "NO Removal Efficiency of Photocatalytic Paving Blocks Prepared with Recycled Materials"; *Construc. Build. Mater.*, **21**, 1746–53 (2006).

[15]F. Mange, P. Couchot, A. Foissy, and A. Pierre, "Effects of Sodium and Calcium Ions on the Aggregation of Titanium Dioxide, at High pH, in Aqueous Dispersions"; *J. Colloid Interface Sci.*, **159**, 58–67 (1993).

[16]B. Zielinska and A. W. Morawski, "TiO_2 Photocatalysts Promoted by Alkali Metals"; *Appl. Catal. B: Environ.*, **55**, 221–6 (2005).

[17]H. Lin, C. P. Huang, W. Li, C. Ni, S. Ismatshah, and Y. Tseng, "Size Dependency of Nanocrystalline TiO_2 on its Optical Property and Photocatalytic Reactivity Exemplified by 2-Chlorophenol"; *Appl. Catal. B: Environ.*, **68**, 1–11 (2006).
[18]S. Brunauer, P. H. Emmett, and E. Teller, "Adsorption of Gases in Multimolecular Layers", *J. Am. Chem. Soc.*, **60**, 309–19 (1938).
[19]E. P. Barrett, L. G. Joyner, and P. P. Halenda, "The Determination of Pore Volume and Area Distributions in Porous Substances. I. Computations from Nitrogen Isotherms", *J. Am. Chem. Soc.*, **73**, 373–80 (1951).
[20]National Institute of Standards and Technology. *NIST X-Ray Photoelectron Spectroscopy Database, Version 3.5*. National Institute of Standards and Technology, Gaithersburg, 2003. Available at http://srdata.nist.gov/xps/
[21]Z. Jingxian, J. Dongliang, L. Weisensel, and P. Greil, "Deflocculants for Tape Casting of TiO_2 Slurries," *J. Eur. Ceram. Soc.*, **24**, 2259–65 (2004).
[22]A. Folli, U. H. Jakobsen, G. L. Guerrini, and D. E. Macphee, "Rhodamine B Discolouration on TiO2 in the Cement Environment: A Look at Fundamental Aspects of the Self-cleaning Effect in Concretes," *J. Adv. Oxid. Technol.*, **12**, 126–33 (2009).
[23]E. Dowty, ATOMS_Software, Kingsport, TN.
[24]Bruker. Bruker_EVA_X-Ray_Diffraction_Pattern_Database, Bruker AXS Inc., Madison, WI.
[25]P. Stefanov, M. Shipochka, P. Stefchev, Z. Raicheva, V. Lazarova, and L. Spassov, "XPS Characterization of TiO_2 Layers Deposited on Quartz Plates," *J. Phys.: Conf. Ser.*, **100**, 1–4 (2008).
[26]Y. L. Lin, T. J. Wang, and Y. Jin, "Surface Characteristics of Hydrous Silica-Coated TiO2 Particles", *Powder Technol.*, **123**, 194–8 (2002).
[27]J. Pouilleau, D. Devilliers, H. Groult, and P. Marcus, "Surface Study of a Titanium-based Ceramic Electrode Material by X-ray Photoelectron Spectroscopy", *J. Mater. Sci.*, **32**, 5645–51 (1998).
[28]A. Iwabuchi, C. Choo, and K. Tanaka, "Titania Nanoparticles Prepared with Pulsed Laser Ablation of Rutile Single Crystals in Water," *J. Phys. Chem. B*, **108**, 10863–71 (2004).
[29]F. Chen, J. Zhao, and H. Hidaka, "Highly Selective Deethylation of Rhodamine B: Adsorption and Photooxidation Pathways of the Dye on the TiO_2/SiO_2 Composite Photocatalyst,", *Int. J. Photoenergy*, **5**, 209–17 (2003).
[30]N. Mandzy, E. Grulke, and T. Druffel, "Breakage of TiO_2 Agglomerates in Electrostatically Stabilized Aqueous Dispersions," *Powder Technol.*, **160**, 121–6 (2005).
[31]Y. Masuda and K. Kato, "Nanocrystal Assembled TiO_2 Particles Prepared from Aqueous Solution," *Cryst. Growth Des.*, **8**, 3213–8 (2008).
[32]B. P. Nelson, R. Candal, R. M. Corn, and M. A. Anderson, "Control of Surface and ζ-Potentials on Nanoporous TiO_2 Films by Potential-Determining and Specifically Adsorbed Ions," *Langmuir*, **16**, 6094–101 (2000).
[33]D. J. Shaw, *Introduction to Colloid and Surface Chemistry*. Butterworths, London, 1966.
[34]D. L. Foulger, P. G. Nencini, and S. Pieri, "Preparation of Anatase Titanium Dioxide," Europe Patent, EP 0722905 A1, 1966.
[35]C. Kormann, D. W. Bahnemann, and M. R. Hoffmann, *Environ. Sci. Technol.*, **25**, 494–500 (1991).
[36]B. V. Derjaguin and L. P. Landau, *Acta Phys. Chim. USSR*, **14**, 633–62 (1941).
[37]E. J. W. Verwey and G. T. J. Overbeek, *Theory and Stability of Lyophobic Colloids*. Elsevier, Amsterdam, 1948.
[38]G. T. J. Overbeek, "The Rule of Schulze and Hardy," *Pure Appl. Chem.*, **52**, 1151–61 (1980).
[39]C. Labbez, B. Jönsson, M. Skarba, and M. Borkovec, "Ion-Ion Correlation and Charge Reversal at Titrating Solid Interfaces," *Langmuir*, **25**[13], 7209–13 (2009).
[40]C. Labbez, A. Nonat, I. Pochard, and B. Jönsson, "Experimental and Theoretical Evidence of Overcharging of Calcium Silicate Hydrate," *J. Colloid Interface Sci.*, **309**, 303–7 (2007).
[41]J. Lyklema, "Overcharging, Charge Reversal: Chemistry or Physics?"; *Colloid Surf. A*, **291**, 3–12 (2006).
[42]B. Jönsson and H. Wennerström, "Ion-Ion Correlations in Liquid Dispersions," *J. Adhes.*, **80**, 339–64 (2004).
[43]L. Guldbrand, B. Jönsson, H. Wennerström, and P. Linse, "Linse, Electrical Double Layer Forces. A. Monte Carlo Study," *J. Chem. Phys.*, **80**, 2221–8 (1984).
[44]B. Jönsson, A. Nonat, C. Labbez, B. Cabane, and H. Wennerström, "Controlling the Cohesion of Cement Paste," *Langmuir*, **21**, 9211–21 (2005).
[45]C. Labbez, B. Jönsson, I. Pochard, A. Nonat, and B. Cabane, "Surface Charge Density and Electrokinetic Potential of Highly Charged Minerals: Experiments and Monte Carlo Simulations on Calcium Silicate Hydrate," *J. Phys. Chem.*, **110**, 9219–30 (2006).
[46]Z. Tang, L. E. Scriven, and H. T. Davis, "Interactions Between Primitive Electrical Double Layers," *J. Chem. Phys.*, **97**, 9258–66 (1992).
[47]J. P. Valleau, R. Ivkov, and G. M. Torrie, "Colloid Stability: The Forces Between Charged Surfaces in an Electrolyte," *J. Chem. Phys.*, **95**, 520–32 (1991).
[48]H. Wennerström and B. Jönsson, "Amphiphile-Water Systems and Electrostatic Interactions," *J. Phys. France*, **49**, 1033–41 (1988).
[49]P. Attard, "Electrolytes and the Electric Double Layer," *Adv. Chem. Phys.*, **92**, 1–159 (1996).
[50]M. Quesada-Perez, E. Gonzalez-Tovar, A. Martin-Molina, M. Lozada-Cassou, and R. Hidalgo-Alvarez, "Overcharging in Colloids: Beyond the Poisson-Boltzmann Approach," *Chem. Phys. Chem.*, **4**, 234–48 (2003).
[51]M. R. Böhmer, Y. E. A. Sofy, and A. Foissy, "Calorimetry of Poly-(Acrylic Acid) Adsorption on TiO_2," *J. Colloid Interface Sci.*, **164**, 126–35 (1994).
[52]Y. F. Houst, P. Bowen, F. Perche, A. Kauppi, P. Borget, L. Galmiche, J.-F. Le Meins, F. Lafuma, R. J. Flatt, I. Schober, P. F. G. Banfill, D. S. Swift, B. O. Myrvold, B. G. Petersen, and K. Reknes, "Design and Function of Novel Superplasticizers for More Durable High Performance Concrete (Superplast Project)," *Cem. Conc. Res.*, **38**, 1197–209 (2008).
[53]G. L. Guerrini, E. Peccati, "Determination of the Degradation of Nitrogen Oxides in the Air by Inorganic Photocatalytic Materials: Continuous Flow Test Method," UNI_11247, Milan, 2009, pp. 1–11.
[54]C. H. Hou, X. Wang, C. Liang, S. Yiacoumi, C. Tsouris, and S. Dai, *J. Phys. Chem. B*, **112**, 8563–70 (2008).
[55]A. F. Wells, *Structural Inorganic Chemistry*, 5th edition, Oxford University Press, Oxford, U.K., 1984.
[56]U. H. Jakobsen, D. R. Brown, R. J. Comeau, and J. H. H. Henriksen, "Fluorescent Epoxy Impregnated Thin Sections Prepared for a Round Robin Test on W/C Determination"; in, *Proceedings of the 9th Euroseminar on Microscopy of Building Materials*, Edited by MATM Broekmans, V. Jensen, and B. Brattli, Norway, 2003.
[57]U. H. Jakobsen, L. Laugesen, and N. Thaulow, "Determination of Water to Cement Ratio in Hardened Concrete by Optical Fluorescence Microscopy"; pp. 27–42 in *SP 191, 2000; Vol. Water-Cement Ratio and Other Durability Parameters: Techniques for Determination*, Edited by M. S. Khan. ACI - American Concrete Institute, Farmington Hills, MI.
[58]F. A. Cotton and G. Wilkinson, *Advanced Inorganic Chemistry*, 5th edition, Wiley-Interscience, New York, U.S.A., 1988.
[59]A. G. Volkov, S. Paula, and D. W. Deamer, "Two Mechanisms of Permeation of Small Neutral Molecules and Hydrates Ions Across Phospholipid Bilayers," *Bioelectrochem. Bioenerg.*, **42**, 153–60 (1997).
[60]A. J. Rutgers and Y. Hendrikx, "Ionic Hydration," *Trans. Farad. Soc.*, **58**, 2184–91 (1962).
[61]H. Binder and O. Zschornig, "The Effect of Metal Cations on the Phase Behaviour and Hydration Characteristics of Phospholipid Membranes," *Chem. Phys. Lipids*, **115**, 39–61 (2002). □